Atmospheric-driven state transfer of shore-fast ice in the northeastern Kara Sea

Dmitry V. Divine,[1] Reinert Korsnes,[2] Alexander P. Makshtas,[3] Fred Godtliebsen,[4] and Harald Svendsen[5]

Received 9 September 2004; revised 19 April 2005; accepted 2 June 2005; published 21 September 2005.

[1] Frequencies of observed occurrences of shore-fast ice in the northeastern Kara Sea for each month during 1953–1990 reveal a multimodality of shore-fast ice extent in late winter and spring. The fast ice extent exhibits mainly three different configurations (modes) associated with the regional topography of coasts and islands. These modes show fast ice areas equal to approximately 98 ± 6, 122 ± 6, and 136 ± 8 1000 km^2. Analysis of the time series of fast ice extent shows that favorable conditions for expansion of fast ice seaward in winter and spring are met if the atmospheric circulation over the northeastern Kara Sea is controlled by the Arctic high, resulting in offshore winds and a significant (up to 6°C) decrease of the monthly mean surface air temperature. In contrast, the penetration of the Icelandic low into the Kara Sea, accompanied by Arctic cyclones coming from the west, is responsible for the partial breakup and decrease of fast ice extent in winter or spring.

Citation: Divine, D. V., R. Korsnes, A. P. Makshtas, F. Godtliebsen, and H. Svendsen (2005), Atmospheric-driven state transfer of shore-fast ice in the northeastern Kara Sea, *J. Geophys. Res.*, *110*, C09013, doi:10.1029/2004JC002706.

1. Introduction

[2] This study proposes and justifies a simplified description of the shore-fast ice extent in the northeastern Kara Sea during late winter and spring (February, March, April, May, and June). The purpose is to estimate, from sparse data, a correlation between atmospheric forcing and formation and breakup of sea ice. The present simplification is in the form of a set of three (idealized) model ice extents. A member from the set of these three model coverages can normally approximate a given extent of shore-fast ice. These model extents are spatially nested in the sense that for any two extents, one either includes the other or vice versa. The physical idea behind these three model coverages is that three distinct groups of islands can stabilize shore-fast ice in the study area. These groups of islands are Sverdrup Island, Izvestiy ZIK islands and Islands of the Arctic Institute, and the Sergei Kirov islands (see Figure 1). One model extent (the smallest) is for when Sergei Kirov islands play a direct role in stabilizing the shore-fast ice extent. Another model extent is for when Sergei Kirov islands, the Izvestiy ZIK islands and the islands of the Arctic Institute (but not Sverdrup Island) stabilize the shore-fast ice. The third model extent (the largest) is for when all of these islands contribute to stabilizing the shore-fast ice.

[3] The present work utilizes this simplification for statistical analysis of atmospheric-driven formation and breakup of shore-fast ice. Such a simplification is also of direct interest for identification of shore-fast ice based on sparse data and available low-resolution satellite imagery. The identification problem is then reduced to distinction among only three possible coverages. Such a simplification should in principle also provide different approaches for statistical and mechanical modeling.

[4] Shore-fast ice is in general a significant feature of ice conditions in the Siberian shelf seas [*Zubov*, 1945; *Timokhov*, 1994]. A belt of immobile ice normally forms along the entire coast of Siberia during winter largely because of its shallowness and numerous islands. The study of fast ice is of interest for several reasons. Massifs, formed by fast ice, complicate the navigation and restrict offshore exploration. The areas of fast ice and adjacent polynyas are the potential suppliers of sediments and pollutants as well as new ice into the Arctic basin. Since fast ice mostly forms in shallow areas, it may take up significant amounts of suspended sediments, especially in the initial stage of ice growth [*Timokhov*, 1994; *Reimnitz et al.*, 1992, 1995; *Eicken et al.*, 1995]. This is of particular importance in estuaries of the great Siberian rivers, which drain huge land areas and industrial zones, thus contributing to the input of pollutants into the shelf seas. The incorporated materials tend to melt out of the ice later in the Greenland and the Barents seas and pollutants may in this way enter the food web there [*Weeks*, 1994; *Pfirman et al.*, 1995, 1997a, 1997b; *Rigor and Colony*, 1997; *Pavlov and Stanovoy*, 2001; *Korsnes et al.*, 2002].

[5] Fast ice normally starts to form in October and it reaches its widest extent during April and May [*Divine et*

[1]Norwegian Polar Institute, Tromsø, Norway.
[2]Norwegian Defense Research Establishment, Kjeller, Norway.
[3]International Arctic Research Center, Fairbanks, Alaska, USA.
[4]Faculty of Science, University of Tromsø, Tromsø, Norway.
[5]Geophysical Institute, University of Bergen, Bergen, Norway.

0148-0227/05/2004JC002706$09.00

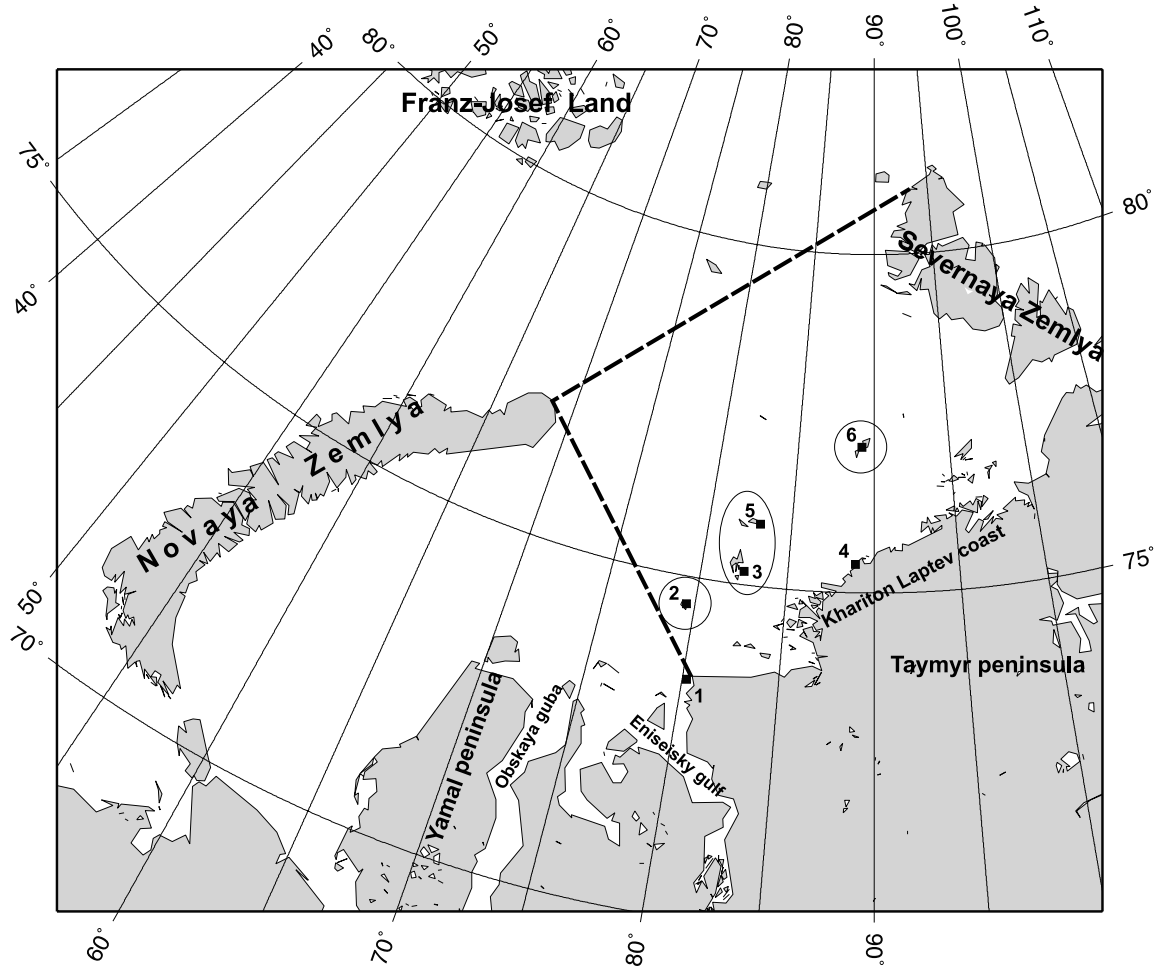

Figure 1. Definition of study area (given by the lines) including the locations of islands referred to in the text: 1, Dikson Island; 2, Sverdrup Island; 3, Islands of the Arctic Institute; 4, Sterlegova Cape; 5, Izvestiy ZIK islands; 6, Sergei Kirov islands. The circles and ellipse highlight the islands that are significant for the anchoring of fast ice.

al., 2004; *Volkov et al.*, 2002]. Largest areas of fast ice tend to form in the northeastern Kara Sea, the Laptev and the Eastern Siberian seas. Fast ice in the Laptev sea, for example, may extend up to 500 km from the shore by the middle of spring [*Dethleff et al.*, 1998].

[6] The present work is about fast ice in the northeastern part of the Kara. The study area is the waters enclosed by a "line" from Dikson Island to Zhelaniya Cape and further to the northern extremity of Severnaya Zemlya Archipelago (see Figure 1). This area of frequent fast ice is rather shallow with a depth less than 25 m. The only exception is near the Severnaya Zemlya Archipelago where the fast ice extent may reach the 100 m isobath.

[7] Our previous studies [*Divine et al.*, 2003, 2004] demonstrated that fast ice in the northeastern Kara Sea undergoes significant seasonal and interannual variations because of changes in the regional weather. Fast ice along the coast of the Taymyr Peninsula can in some situations be almost absent while in other instances it can reach up to 250 km from the shore. The present work shows that these variations are discrete and associated with the topography of islands in the region. Significant changes of the fast ice extent during winter or spring normally take place during short periods where large areas form or breakup.

[8] Section 2 below briefly introduces the data used in the present study. Section 3 shows modes of fast ice extent derived from its frequency of occurrence. Section 4 correlates atmospheric circulation patterns with occurrence of and transitions between different modes of fast ice. Section 5 gives final assessments of these analyses.

2. Data

[9] A detailed description of the data sets and data handling for this study is given by *Divine et al.* [2004]. Russian historical ice charts for the Arctic marginal seas compiled by the Arctic and Antarctic Research Institute (AARI) provide information about extents of different types of sea ice. We use information about fast ice in the Kara Sea from the data set "AARI 10-day Arctic Ocean EASE-grid sea ice observations," which is available via the EOSDIS NSIDC Distributed Active Archive Center (NSIDC DAAC), University of Colorado [*Fetterer and Troisi*, 1997]. There are data from 523 observation campaigns

(here called "surveys") for ice conditions in the whole study area during 1953–1990. This includes 42, 40, 46 and 73 surveys of fast ice for March, April, May and June, respectively. Each survey is attributed to one of three 10-day periods of the month when the survey was made. We will refer to this data set as "the AARI data set." The grid spacing in the AARI data set is 12.5 km. The summing of pixel areas constituting fast ice gives the estimate of the fast ice area for every particular survey. The accuracy of determination of the boundaries between different types of sea ice with AARI ice maps lies between 2 and 10 km [*Fetterer and Troisi*, 1997]. However, we use the gridded data set, so the actual boundaries of fast ice should be somewhere within the spacing between given grid points (or pixel). Hence the relative error for a given area of the fast ice is less than:

$$\delta S = \frac{N_b}{2N} \tag{1}$$

where N_b and N are the number of pixels on the border of fast ice and total number of pixels in the fast ice area, respectively. Analysis shows that the error in estimating the fast ice area in the northeastern Kara Sea in March-May is around 7.5% [*Divine et al.*, 2004].

[10] The frequency of occurrence of fast ice $P(z)$ is given for each grid point z as the ratio of the number of observations with fast ice (N_{fi}) and the total number (N_{tot}) of valid observations at z:

$$P(z) = \frac{N_{fi}(z)}{N_{tot}(z)} \tag{2}$$

Divine et al. [2004] show an example of the monthly frequencies of occurrence of fast ice, but $P(z)$ can be defined for any given set of surveys.

[11] Two other data sets provide a 14 years extension of the time series of the AARI data. We use DMSP SSM/I daily polar gridded brightness temperatures [*Maslanik and Stroeve*, 1990 updated 2003] from NSIDC DAAC for estimation of the shore-fast ice extent. The analysis was made for the period 1991–1996 using a method developed by [*Divine*, 2003]. We use new AARI ice charts for the most recent 8 years of the study period. These weekly ice charts are publicly available electronically in the form of GIF images at the AARI Web site (http://www.aari.nw.ru). These data are based on infrared satellite images and spaceborne radar data. This is the common method for observations for the last 10 years of the AARI data set. We carried out a detailed statistical analysis of the AARI data for 1953–1990, while the latter two data sets were subject to visual inspection as described further in section 3.

[12] To analyze the atmospheric forcing on fast ice, we used the National Center of Environment Prediction (NCEP) Reanalysis data provided by the NOAA-CIRES Climate Diagnostics Center, Boulder, Colorado, USA, from their Web site (http://www.cdc.noaa.gov) and the twice-daily Northern Hemisphere extratropical cyclone data set provided by the NSIDC [*Serreze*, 1996]. The first one provides daily SLP data, continuing from 1948, on a 2.5° latitude/longitude grid. The second data set comprises a 28-year record (since May 1966) of cyclone statistics on a 47 × 51 Octagonal grid. We also used the archive of weather observations at the Dikson Island meteorological station. These observations are available for each 6 hours during 1950–1965 and for each 3 hours during 1965–1990. Daily average surface air temperatures during 1950–1990 on a 1.9° latitude/longitude grid for the Northern Hemisphere were derived from the respective 6-hour data provided by the NCEP Reanalysis.

3. Modes of Fast Ice in the Northeastern Kara Sea

[13] Two significant features appear to be present in the spatial distribution of the frequency of occurrence of shore-fast ice in the northeastern Kara Sea during spring [*Divine et al.*, 2004].

[14] The first apparent feature of this distribution is an increased probability for fast ice to exist from the southwest to the northeast along the western coast of the Taymyr Peninsula, from Dikson Island to Severnaya Zemlya (see Figure 3 of *Divine et al.* [2004]). The distance of the fast ice border from the shore varies within a range of 12–50 km (about 1–4 times the length between data grid points). The most significant variations of the fast ice extent are therefore due to its expansion and retreat along the shore line.

[15] The second apparent feature is the discrete change in positions of the southwest border of fast ice. A visual inspection of fast ice maps reveals that its southwest border tends to occupy one of three positions: between Sergei Kirov islands and the Laptev's coast, the islands of Izvestiy ZIK, the Arctic Institute and the western Laptev's coast, and between Sverdrup and Dikson islands (see Figure 1).

[16] The statistical approach below confirms the above assessment. This approach includes a grouping of available surveys of shore-fast ice according to the following procedure: If the shore-fast ice extent reaches the Sergei Kirov Islands but not the Izvestiy ZIK Islands, the Islands of the Arctic Institute and Sverdrup Island, then it is classified as Group 1 (S). Group 2 (L_1) is for situations when the shore-fast ice reaches the Sergei Kirov islands, the Izvestiy ZIK Islands and the Islands of the Arctic Institute, but not Sverdrup Island. Group 3 (L_2) is for situations when the shore-fast ice reaches all these islands. Each of these islands or island groups presumably contribute to stabilizing the shore-fast ice when it reaches them.

[17] A few of the surveys cannot be classified into these three groups. One may interpret these situations as events with unstable shore-fast extents.

[18] Figure 2 shows the spatial distribution of the frequency of occurrence (equation (2)) for these three groups of shore-fast ice for the four spring months March-June. The figure shows that the above classification procedure groups the shore-fast ice extents into three groups with small variations within each group. Hence one can consider that the procedure gives a natural classification reflecting that there are only a few stable configurations of shore-fast ice. Any random classification would not give such small variation within each group. Figure 2 also shows the 5%, 50% and the 95% isolines of the frequency of occurrence. The 50% isoline here defines the median ice extent, while the 5% and the 95% isolines outline the area of the possible

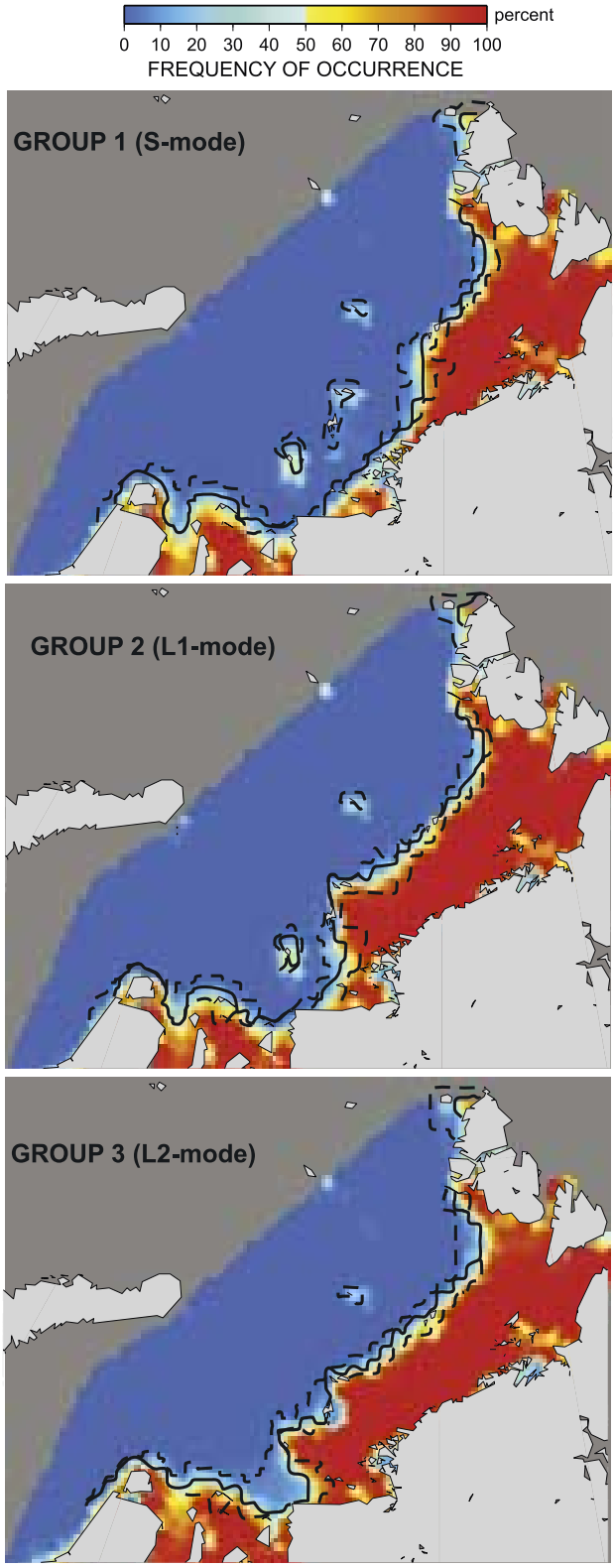

Figure 2. Frequency of occurrence of shore-fast ice for the three groups of surveys during March–June (S, L_1, and L_2 modes). Figure is based on the AARI ice charts 1953–1990. The 50% isoline for each of these distributions defines the median fast ice border within each group (solid lines). The dashed lines similarly delineate the isolines with the 95% and 5% frequencies of occurrence.

positions of the fast ice edge for each group. Caution must be exercised not to make a direct physical interpretation of the "median" shore-fast extent other than that the shore-fast extent normally is close to this (within each group) since the area of variation is relatively small.

[19] Clustering of fast ice area around the typical areas for the (above) three classes of fast ice extent supports the significance of this classification. The SiZer technique [*Chaudhuri and Marron*, 1999] is known to be efficient for identifying clustering via estimates of probability density functions (PDF). A regular histogram is common to estimate nonparametric probability density functions from data. This approach gives a tradeoff between resolution (bin size) and uncertainty. A more general SiZer technique is better for use in identifying multiple local maxima, which are typical of probability distributions for mixed populations. Figure 3 (upper panel) shows estimates of the PDF from a SiZer analysis based on areas of fast ice from the AARI data for March-June 1953–1990. These estimates are from application of the Gaussian kernel density estimator as described by *Chaudhuri and Marron* [1999]. A kernel width parameter h defines the smoothness of the probability density estimates. The positions of green circles in the upper panel of Figure 3 represent observed areas of shore-fast ice during the period March-June for 1953–1990. The blue lines show density estimates for various values of h. This gives a multiresolution view of the data. The degree of smoothness of these different estimates increases with increased h. The red line represents a density estimate where the kernel width h has a value of 0.55 according to the choice of *Sheather and Jones* [1991]. The SiZer plot (lower panel in Figure 3) shows the derivative behavior for the PDF estimate for a particular h For each location (x, h), a test is performed to see whether the derivative is significantly different from zero. Blue, red and purple highlight the (x, h) locations with significantly positive, negative and zero derivatives, respectively. The solid horizontal line in the lower panel, corresponds to the *Sheather and Jones* [1991] choice for h.

[20] Grey shows locations where there is not enough data for proper inference. Figure 3 shows that for h equal to 0.55 this is the case for areas (x) less than 83,000 km^2. The curve has a positive derivative for x in the range 83,000–94,000 km^2. It has single peaks for x at 98,000 km^2 and 125,000 km^2. These peaks show clustering of fast ice area around these values. However, the present SiZer estimates do not reveal separate clusters of area that can be explained by different typical spatial configurations (Group 2 and Group 3). Our estimates show, that the variability of the seaward border of fast ice may mean these groups of fast ice have overlapping ranges of likely area (i.e., area alone does not characterize these two different configurations).

[21] Table 1 shows the (conditional) monthly mean and standard deviation of the area of observed fast ice within each group (based on the AARI data) for March-June. It demonstrates that about 85% of the available surveys during March-June fall into the present classification scheme. The fraction of the unclassified surveys varies from 9% in May to 15% in March and April.

[22] The spatial configuration of the median ice border agrees well with the prevalent observed positions of the fast ice borders to within 1–2 data grid points (12.5 to 25 km)

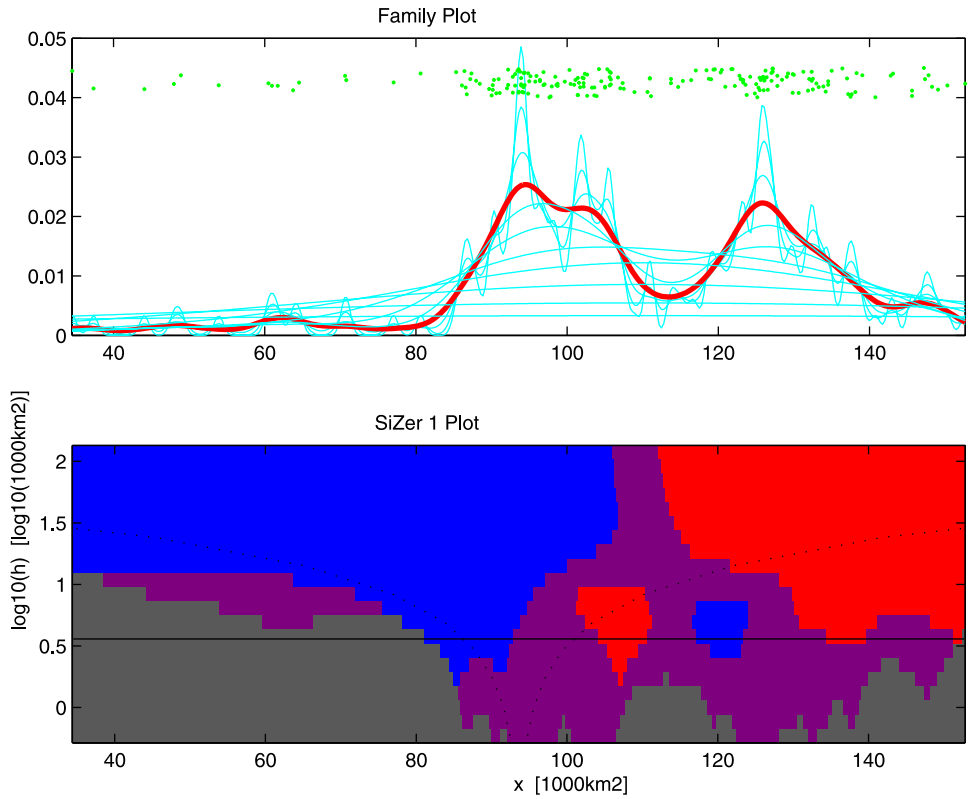

Figure 3. (top) Circles, area of shore-fast ice in the northeastern Kara Sea during March-June; lines, estimates of the probability density function (PDF) for different values of the bandwidth h. (bottom) SiZer significance test at 95% confidence level for the PDF. Color coding: purple, no significant trend; blue, significant increase; red, significant decrease; gray, insufficient data. The dotted curves show "effective window widths" for each bandwidth, as intervals representing $\pm 2h$. The thin solid horizontal line at h equal to 0.55 is for the kernel width according to the choice of *Sheather and Jones* [1991]. See also text for detailed explanation of the figure.

on the seaward side of fast ice and 1–4 data grid points on its western boundary. This allows consideration of these features as "modes" of shore-fast ice in the northeastern Kara Sea. The general description of the modes is given below.

[23] The first mode, referred to below as the "S mode," is smallest and its main area lies between the Severnaya Zemlya Archipelago and the "line" between the Sergei Kirov Islands and Sterlegova Cape. This mode represents, with a few exceptions, the smallest possible extent of fast ice under any condition. We identified, for the period 1953–1990, 19, 16, 18 and 31 surveys in March, April, May and June, respectively, conforming to this S mode.

[24] The second mode, L_1, is associated with the expansion of fast ice further to the southwest to the "line" between the Islands of Izvestiy ZIK, the Islands of the Arctic Institute and the western bound of Khariton Laptev's coast. We identified 11, 8, 10 and 18 surveys in March, April, May and June, respectively, conforming to this mode.

[25] The third mode, L_2, represents the largest extent of fast ice encompassing the area between Sverdrup Island and the Severnaya Zemlya Archipelago. This mode was realized 6, 10, 14 and 15 times in March, April, May and June, respectively. Note, that we assign the same symbol "L" to the second and the third groups of surveys, thus underscoring that they are not discriminated on the PDF.

[26] There have been special events where fast ice has continuously covered both this area and the area outside the Ob and Yenisei estuaries. Such events were observed during the second 10-day periods of April and May 1964 and the first 10-day period of April 1979. The area of fast ice in the northeastern Kara Sea was as large as 150,000 km^2 during these events which can be considered as an extreme realization of the L_2mode.

Table 1. Average Fast Ice Areas, Their Standard Deviations, and the Respective Relative Frequencies of Realization for Each Group of Surveys Associated With One of Three Classes of Fast Ice Extent in the Northeastern Kara Sea[a]

Month	Group 1 (Mode S)	Group 2 (Mode L_1)	Group 3 (Mode L_2)
March	94 ± 5 (0.45)	125 ± 4 (0.26)	132 ± 10 (0.14)
April	97 ± 5 (0.40)	120 ± 7 (0.20)	135 ± 8 (0.25)
May	98 ± 6 (0.39)	124 ± 4 (0.22)	137 ± 8 (0.30)
June	96 ± 6 (0.42)	122 ± 7 (0.25)	136 ± 8 (0.21)
March-June	98 ± 6 (0.40)	122 ± 6 (0.23)	136 ± 8 (0.22)

[a]Average fast ice area values are in 1000 km^2, and respective relative frequencies of realization are given in parentheses. Table is based on the AARI ice charts of 1953–1990.

Table 2. Seasonal (February–June) Number of Surveys of Fast Ice in the Northeastern Kara Sea Assigned to the S Mode or One of the L Modes[a]

Year	S Mode	L Mode	Prevalent Mode
1953	2		S
1954	3		S
1955	2		S
1956	3		S
1957		3	L
1958		3	L
1959		4	L
1960	3		S
1961	3		S
1962	3		S
1963	4		S
1964	1	3	L
1965		3	L
1966	1	2	L
1967		7	L
1968	7		S
1969		7	L
1970	1	6	L
1971	1	6	L
1972	4		S
1973	2	4	L
1974		4	L
1975		7	L
1976	7		S
1977	8		S
1978	4	4	L
1979	2	4	L
1980	1	5	L
1981	1	9	L
1982	8		S
1983	9	1	S
1984	6	5	S
1985	13	1	S
1986	10	1	S
1987	8		S
1988	6		S
1989	6	1	S
1990	2	2	L
1991			
1992	4	6	S
1993	9		S
1994		6	L
1995			
1996	2	2	S
1997	13	2	S
1998	14		S
1999	3	15	L
2000		17	L
2001	2	14	L
2002			U
2003	13	3	S
2004		14	L

[a]S and L in the fourth column denote the prevalent mode. The 1991 and 1995 data were missing.

[27] We were unable to classify 6 surveys for March, 6 for April, 4 for May and 9 for June. These are mostly events where the shore-fast ice appear as patches along the mainland along the entire northeastern Kara Sea shore and with total area less than 80,000 km^2. Four cases demonstrate intermediate ice extent between the S-mode and L_1-mode position of the southwest border of fast ice.

[28] Visual inspection of surveys from January, February and July reveals that data for February fall well within the proposed classification, though the fraction of unclassified observations is large for February (25%). The fraction of unclassified surveys is even larger for January and July (respectively 65% and 75%).

[29] Unclassified surveys in January and February typically show initial stages of fast ice growth starting from close to the shore. The fast ice extent has in such situations not yet reached a stable configuration where it tends to stay over time. It seems also often to be unstable in July, and especially in the second and third 10-day periods of July. This is a typical time for fast ice to start to break up [*Divine et al.*, 2004], and the mechanisms controlling its extent are different from the rest of the year.

[30] Note that the present proposed classification is spatial rather than spatial-temporal as suggested by *Borodachev et al.* [2000]. It means that the development of fast ice throughout the season can be viewed as a chain of transitions between modes, at least within the period February-June when this approach is valid.

4. Atmospheric Circulation Patterns and Shore-Fast Ice in the Kara Sea

[31] This section shows relationships between dominating atmospheric circulation patterns and the extent of shore-fast ice in the Kara sea. Table 2 shows the number of observations of fast ice in the study area during February-June identified as the S mode or one of the L modes. The L mode of fast ice during February-June dominated the years 1957–1959, 1964–1967, 1969–1971, 1973–1975, 1978–1981, 1990, 1994, 1999–2001 and 2004 (hereinafter called "L-mode years"). The S mode dominated in 1953–1956, 1960–1963, 1968, 1972, 1976, 1977, 1982–1989, 1992, 1993, 1996–1998 and 2003 (hereinafter called "S-mode years"). Three particular years (1978, 1990 and 1996) have the same number of surveys with S and L configurations of fast ice. They are considered as L-mode years, however, since S modes always preceded L modes during the winter, i.e., fast ice showed a tendency to expand and finally reached the maximum possible extent.

[32] Figures 4 and 5 show isolines of monthly mean sea level pressure (SLP) for these groups of years in the western Barents, the Kara and the eastern Laptev Sea. Figure 6 shows differences between these mean pressure fields.

[33] Figures 4 and 5 illustrate that in years when the fast ice extent was relatively large (L modes) the sea level air pressure was high compared to years with smaller extent of fast ice (S mode). The difference can be as high as 6 mbar depending on the month and place, which is clearly demonstrated in Figure 6. The most noticeable feature in the distribution of the SLP difference is a formation of a high-pressure anomaly over the Kara Sea. The position of the center of the pressure anomaly varies and changes from the Taymyr Peninsula in the southeast in February to Franz Josef Land in the northwest in April. This high-pressure center can play the role of a barrier for cyclones tending to bring mild Atlantic air into the interior of the Kara Sea. We can also expect that enhanced westerly flow occurs across the Kara Sea in years when the fast ice extent is relatively small.

[34] Easterly flow related to a lasting high pressure is common for years of relatively large fast ice extent. This is consistent with our previous results [*Divine et al.*, 2003, 2004] demonstrating that westerly and southwesterly sur-

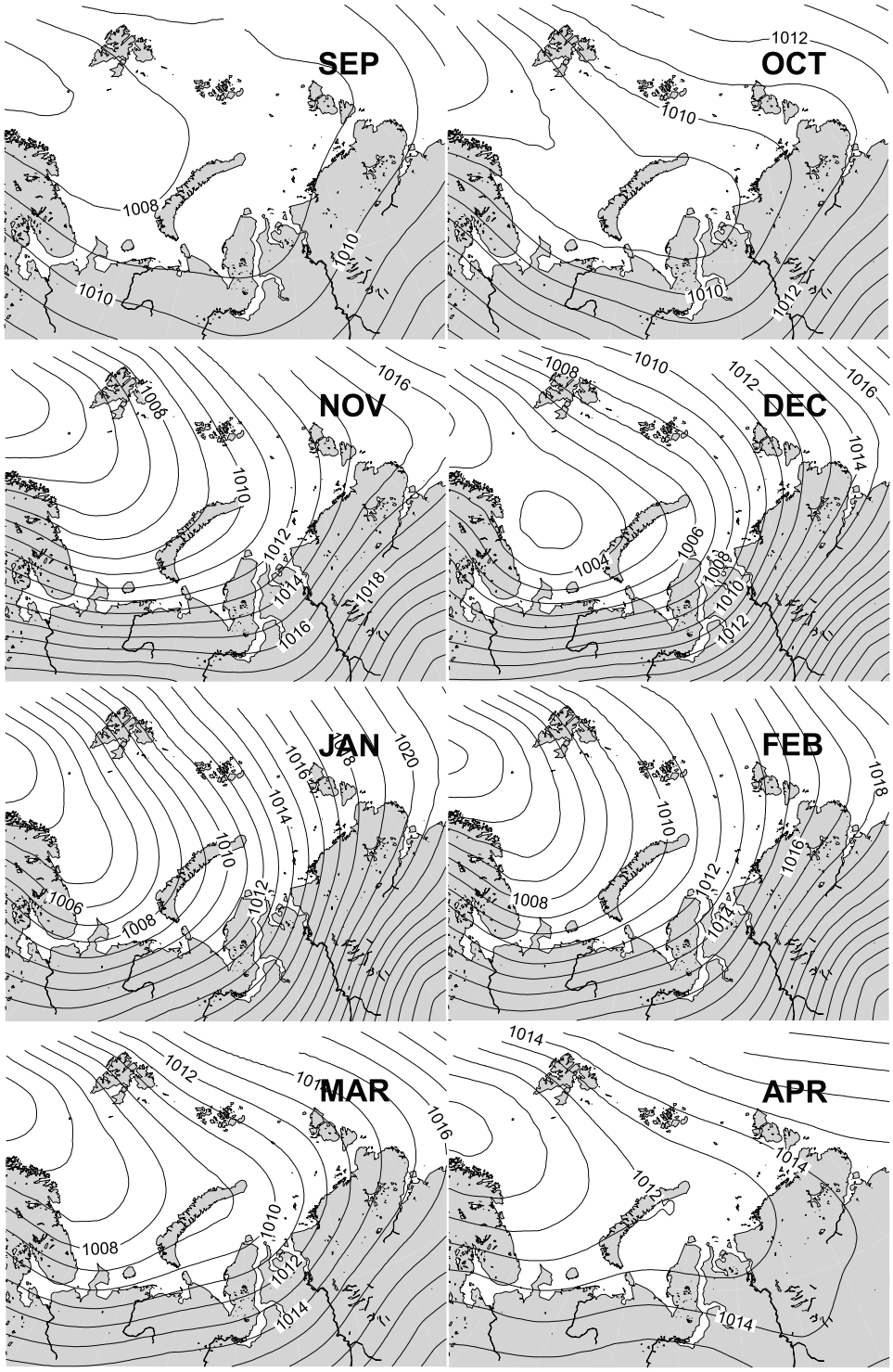

Figure 4. Mean sea level pressure for September–April for S-mode years.

face winds and relatively high temperature tend to give smaller fast ice area. *Rogers and Mosley-Thompson* [1995] demonstrated similar relationships between surface air temperature anomalies and sea level pressure patterns in the Kara Sea.

[35] A study of the cyclone data set indicates an increase of cyclone activity in years with prevalent S mode of fast ice in the northeastern Kara Sea. These cyclone records start at 1969. We therefore in this study selected the 10 last L-mode years from the above list of 15 ''L-mode years'' and similarly we selected 10 S-mode years. We then calculated, for each of these two sets of 10 years, the mean number of cyclones registered at each cyclone data grid node within the study area during September-April. Figure 7 shows that the number of cyclones tracked through the Kara Sea during the fall-spring season was from 10 to 14 when the

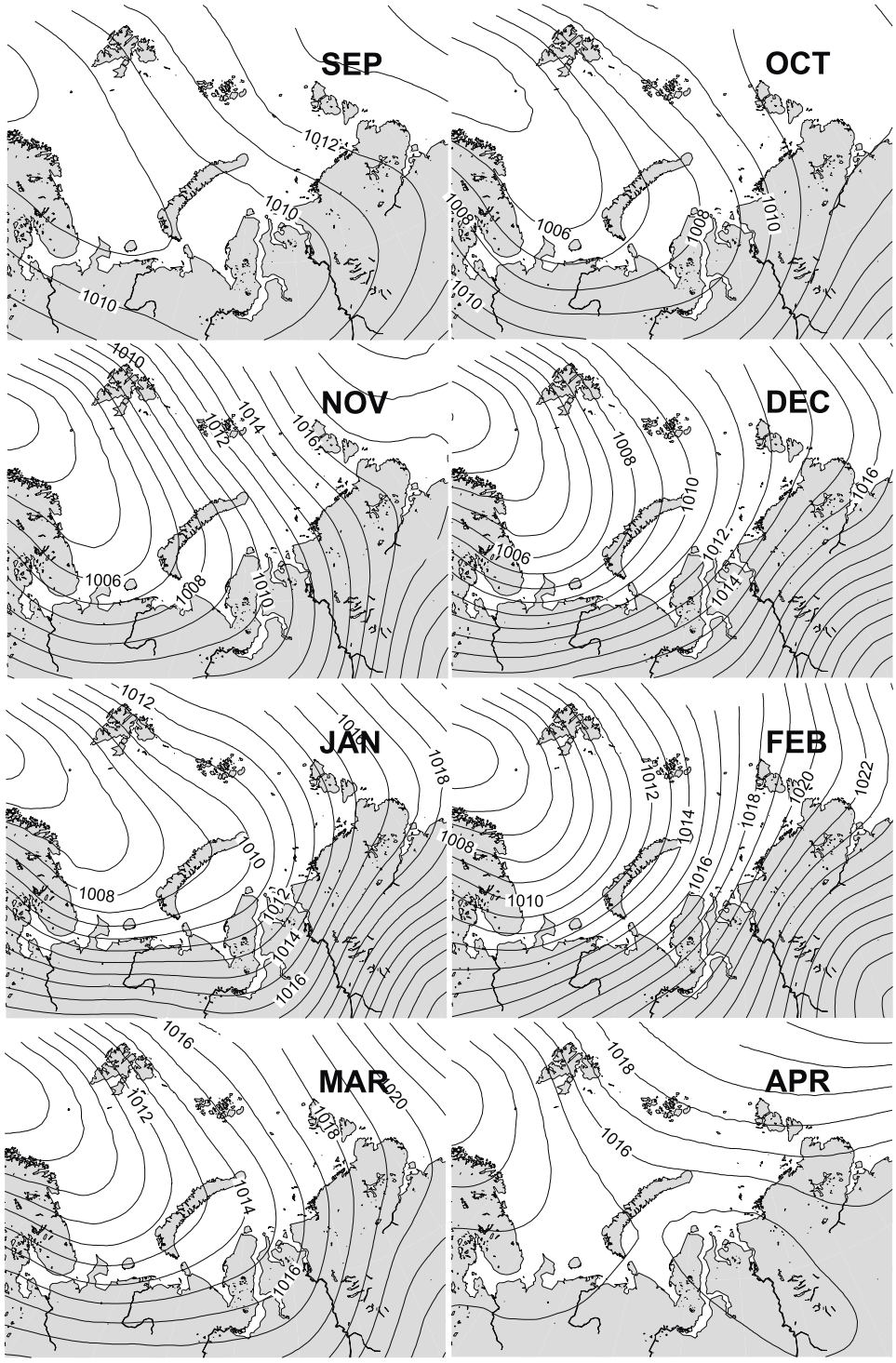

Figure 5. Mean sea level pressure for September–April for L-mode years.

S mode of the fast ice dominated, while this number was between 8 and 12 when one of the L modes dominated.

[36] The analysis of the time series of fast ice area revealed that the growth of fast ice in winter and spring is nonuniform with events of quick expansion seaward and partial breakups. Those cases of changes in fast ice extent configuration, where the corresponding change in fast ice area was more than double the uncertainty, were selected for further analysis. The increase of the area of fast ice can be as high as 300% within a month. Such events were identified in January-April of 1964, 1966, 1968, 1970, 1971, 1978, 1980, 1981, 1984–1986, 1989 and 1997–2002 (34 events in total during 1953–2004). We also identified 16 events of fast ice breakup during the winter (October 1984, December 1983, March and April 1985, April 1988 and May 1989, March 1997, 1998, 2000, 2001, 2003, January 2001, 2002, April 2003). The fast ice cover after the breakups could take configurations typical for the earlier stages of its formation,

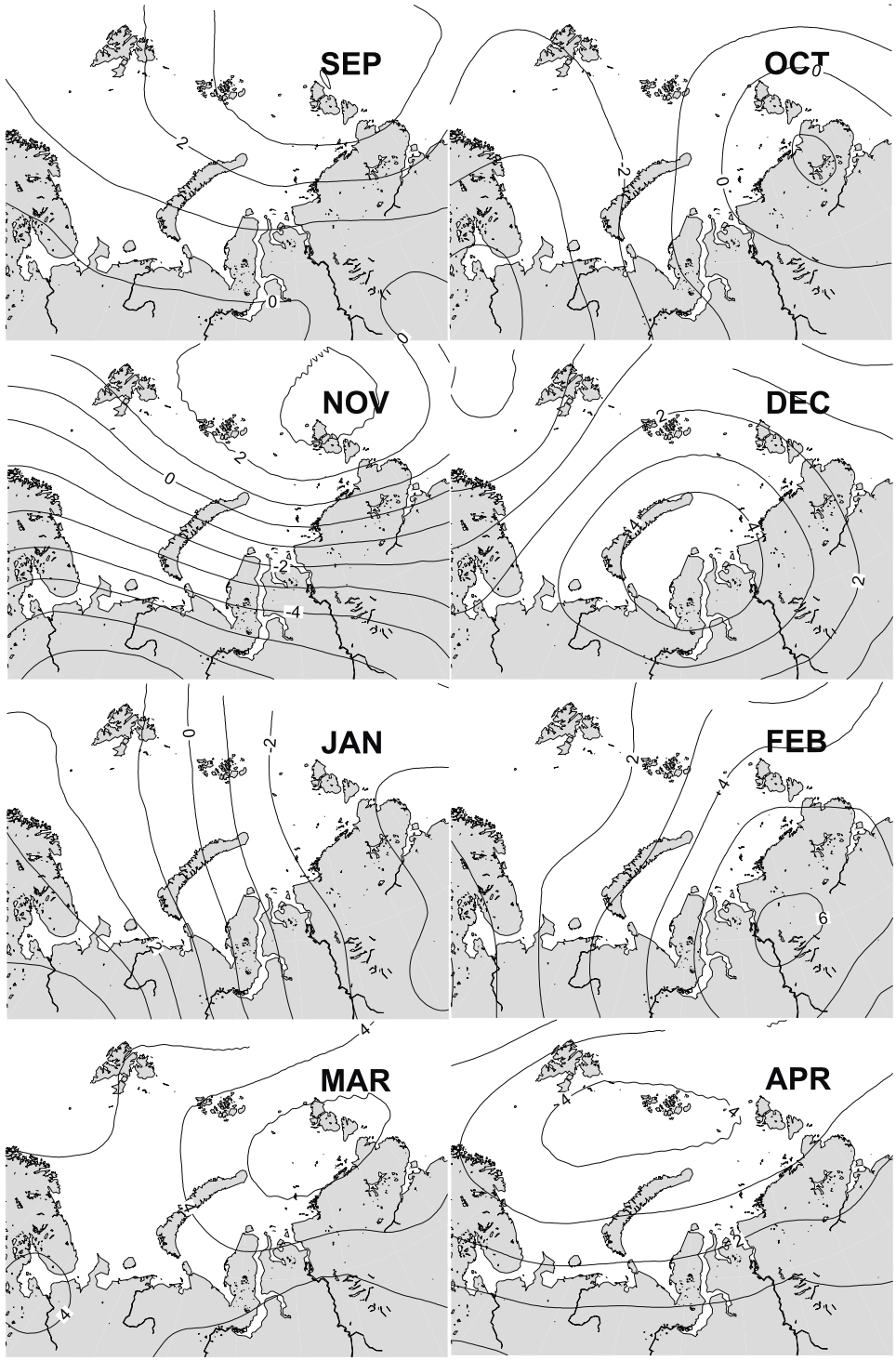

Figure 6. Mean difference between sea level pressure for L-mode years and S-mode years (for September–April).

for example, patches of fast ice along the coast of the Taymyr Peninsula.

[37] As a period of fast ice transformation we define a time interval between the two neighboring surveys with different configurations of fast ice. The typical values for the AARI data are 20 days (two surveys attributed to the neighboring 10-day periods) or 30 days (two surveys within a month). The contemporary observations are available on a weekly basis, so the transformation period amounts to 14 days.

[38] Figure 8 shows mean sea level pressure (SLP) for events of fast ice growth and partial breakups. The upper part of this figure shows mean SLP for 8 periods when fast ice transformed from S mode to L_2 mode and two transformations from L_1 mode to L_2 mode. These events were during February–March 1968, March–April of 1964, 1966

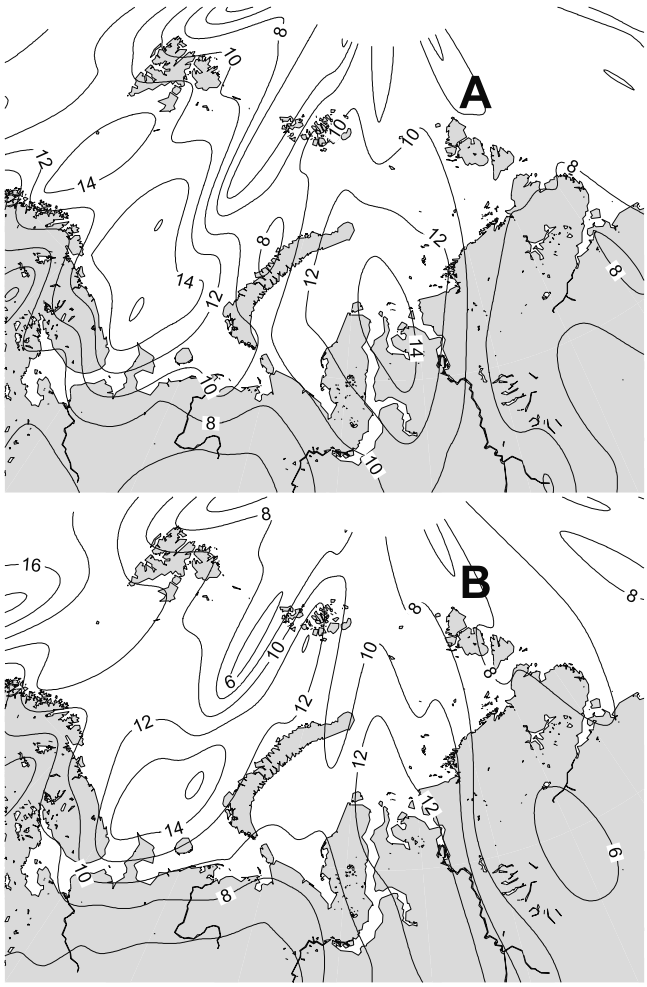

Figure 7. Mean number of recorded cyclones during September–April for (a) 10 S-mode years and (b) 10 L-mode years.

and 1979, April–May 1971 and 1981, February 1998, March 1999 and 2001, December and January 2000. The Figure 8a illustrates a SLP pattern, which is especially favorable for a quick expansion of fast ice in the northeastern Kara Sea. The middle part of Figure 8b shows the same type of result which comes from a larger data set (mean SLP for 42 different cases when the fast ice extent expands in any way).

[39] The illustration demonstrates that fast ice tends to expand during periods of high sea level pressure over the entire Kara Sea, reaching 1020–1024 mbar in its northeastern part. The orientation of isobars to the northeast suggests that the atmospheric circulation in the study area was controlled by the Arctic high and that offshore winds from between East and South were prevalent in the whole Kara Sea and in that way eliminating the ice drift from the western Kara Sea compressing fast ice in the northeastern Kara Sea.

[40] Figure 8 also illustrates that fast ice tends to break up when there is deep penetration of low-pressure systems, originating in the North Atlantic, into the Kara Sea area. The net mean pressure difference between the cases of fast ice expansion and breakup was from 8 to 10 mbar in the southwestern Kara Sea while in the northeastern Kara Sea it exceeded 14 mbar.

[41] Figures 8a and 8b show characteristic sea level air pressure patterns that were present within a period for 33 out of the 42 cases of fast ice growth.

[42] Records of surface air temperatures at Dikson Island during winter show specially cold periods lasting more than 5 days. The temperature during these periods can stay below the climate mean minus one standard deviation for the given time of the year. Such cold periods accompanied 36 out of 42 events of fast ice growth.

[43] Figure 9 shows spatial distributions of mean surface air temperature during cold periods longer than 5 days at Dikson Island for January, February, March and April (i.e., mean temperature for such cold periods with associated fast ice expansion). The figure shows low temperatures in the entire northeastern Kara Sea. This seems to be a typical situation when fast ice forms and reaches stable and lasting configurations.

5. Discussion and Conclusions

[44] This study shows that fast ice in the northeastern Kara Sea tends to form and remain in one of three spatial configurations (modes), distinguished by the expansion of the ice border to the southwest along the coast of the Taymyr Peninsula. These modes of fast ice are spatially nested. The southwest border of fast ice for the smallest of these stable extents (S mode) passes between the Sergei Kirov Islands and Sterlegova Cape. The intermediate stable state (L_1 mode) reaches in the southwest to the line between Izvestiy ZIK, the Arctic Institute islands and the western boundary of Khariton Laptev's coast. The largest stable extent (L_2 mode) encompasses the area around Sverdrup Island.

[45] The proposed classification is valid during February-June and covers about 85% of all available surveys. Fast ice seems typically not to reach any stable configuration during December and January [*Divine et al.*, 2004], and hence the extent during this time is more unpredictable compared to February–June when it is not so sensitive to typical atmospheric forcing. The fast ice extent typically starts to be unstable again in July giving a similar sensitivity to external forcing and more unpredictable behavior.

[46] Islands seems to play a key role in formation and stabilization of fast ice in the northeastern Kara Sea. Mechanical simulations of fast ice breakup due to wind stress support this suggestion [*Zyryanov et al.*, 2002].

[47] Multimodal behavior of fast ice in the northeastern Kara Sea means that the fast ice area characterizes its spatial configuration quite well. Another result of our findings is that one should be cautious about using the term "average" with reference to the extent of fast ice in the northeastern Kara Sea. Any definition of an "average" or "median" for the fast ice extent in the northeastern Kara Sea may not reflect any physically stable (and potentially lasting) or physically realistic configuration. The direct average of fast ice area for spring months over several decades yields a value which lies between the area for the S mode and the L_1 mode. Statistical methods taking into account possible stable configurations may support better interpretations and give more reliable pre-

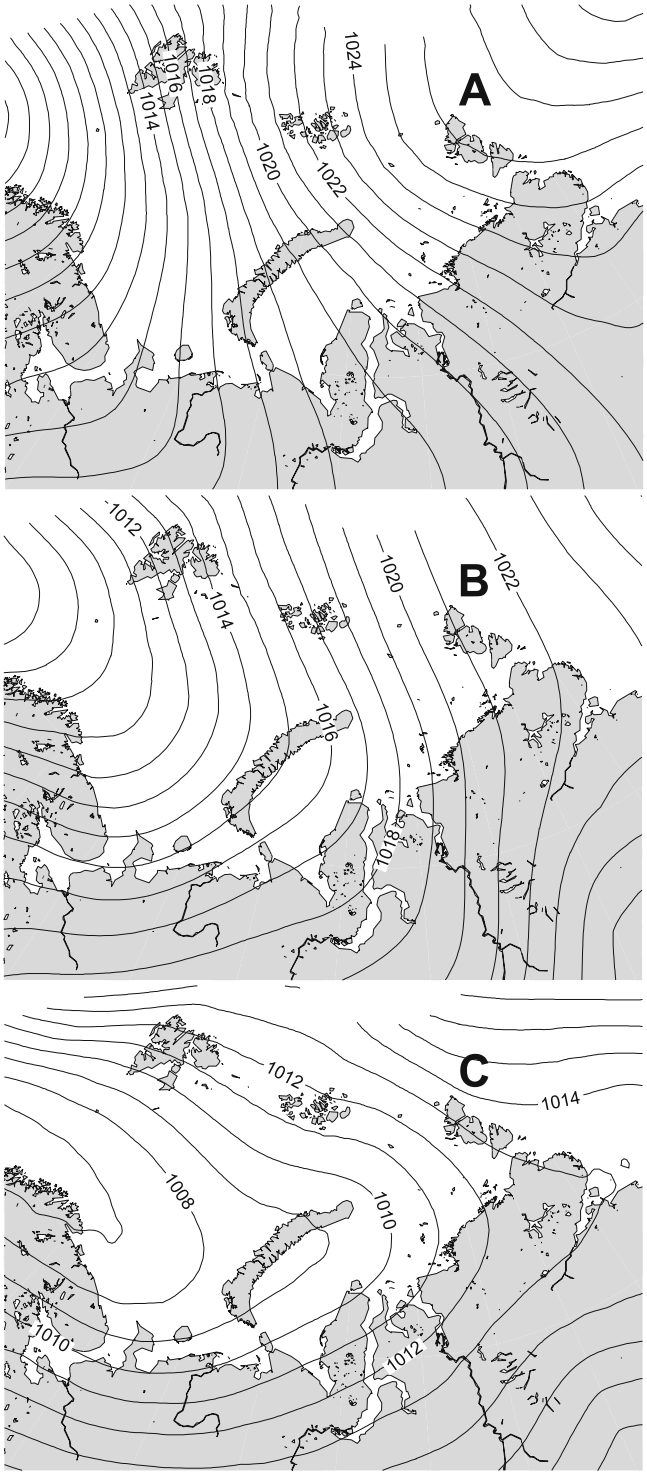

Figure 8. Mean sea level pressure for periods with events of fast ice expansion or partial breakup. (a) Ten periods with change from S mode to L_2 mode and two periods with change from L_1 mode to L_2 mode. (b) Forty-two periods with events of any fast ice expansion. (c) Sixteen periods with partial breakup of fast ice in winter or spring.

dictions. One may assume that at points/situations of instability, small variations of forcing can give large "random" or much unpredictable variations of the area of fast ice extent. It takes time for fast ice to form into a stable configuration after, for example, a storm has broken it up, and during such periods the sensitivity to wind and temperature may be extra large. The transfer between modes has partly an intrinsic mechanical component in the way that a large extent may transform into a temporary much smaller extent when it breaks (even if succeeding wind and temperature conditions favor a larger extent). It may therefore sometimes give simpler physical interpretations if one, for example, tries statistically to relate climate parameters to lasting modes of fast ice extents.

[48] Large extents of shore-fast ice (L modes) tend to appear during periods of high pressure. The presence of the high air pressure over the Kara Sea hinders the penetration of Arctic cyclones from the west into the Kara Sea. A subsequent drop of surface air temperatures and wind speeds favors the growth of fast ice [*Divine et al.*, 2004].

[49] Specific patterns of sea level pressure were found to accompany the process of fast ice growth or destruction. Growth was preferentially observed when the northeastern part of the Kara Sea was controlled by the Arctic high. Deep penetration of low-pressure systems into the Kara Sea interior, in turn, occurred in all cases with observed partial breakup of fast ice during the spring.

[50] Specially low surface air temperatures were observed in the entire northeastern Kara Sea during fast ice growth events. Such cold periods, lasting more than 5 days, are accompanied by offshore winds from between east and south, and are especially favorable for expansion of fast ice. This is well demonstrated by a correlation of close to 0.7 between the area of fast ice in May and the respective accumulated freezing-degree days.

[51] Periods of low temperature can be significant for closing of the polynya outside the fast ice area, as well as for the formation of young ice at its border. According to the estimates of *Pease* [1987], the maximum polynya width and opening time in the Bering Sea are sensitive to the meteorological conditions, and especially to the surface air temperature. Surface air temperatures during January-April in the study area are typically between $-25°C$ and $-15°C$ and wind velocities are about $5-10$ m s^{-1}. The opening time is in this case within $50-100$ hours. For surface temperatures around $-30°C$ a polynya stays open for 40 hours, while at $-40°C$, because of the exponential nature of the governing equation, the time decreases to about 20 hours.

[52] Despite the relative simplicity of this model and uncertainties due to extrapolation of the results obtained for the Bering Sea to the Kara Sea, the order of magnitude of these estimates should still be valid. One should therefore expect that there are two processes to accompany periods of offshore winds and significant temperature drops: freezing over the polynya with subsequent integration of young ice into fast ice and incorporation of frazil ice swept under the edge of fast ice by the wind-induced convection [*Kozo*, 1983]. Conversely, under severe temperature conditions related to events of onshore winds, incorporation of drift ice into the fast ice may occur. Any of these processes eventually lead to the expansion of the fast ice area.

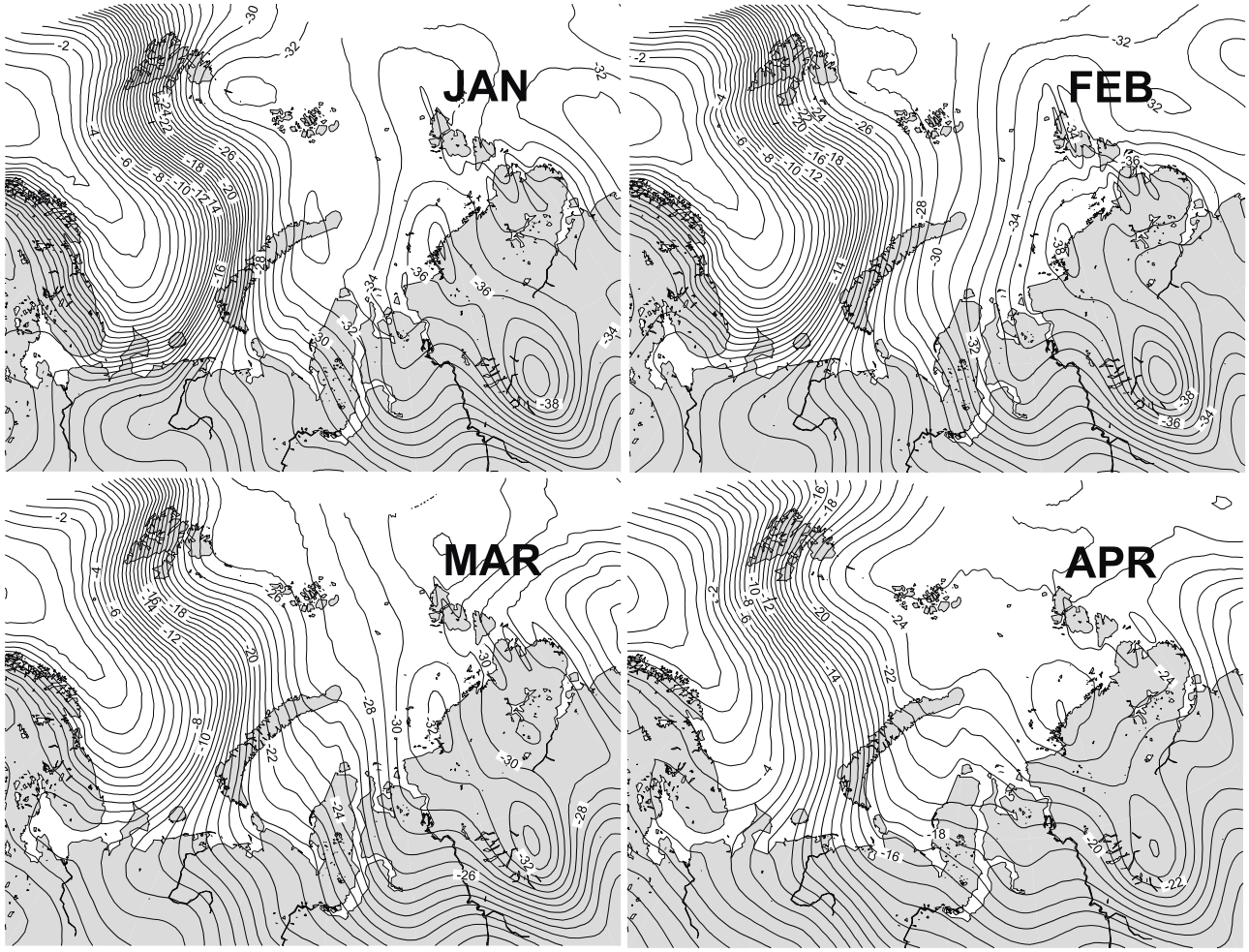

Figure 9. Spatial distributions of mean surface air temperature during cold periods with fast ice expansion for January–April. See text.

[53] The present discrete view of shore-fast ice in the Kara Sea (i.e., the present classification into three different modes) may be used within various statistical analyses. Table 2 shows that modes of fast ice in the Kara Sea tend to cluster in the way that a year where the S mode dominates, tend to be followed by another S-mode year, and similarly one L-mode year tends to be followed by another.

[54] A simple frequency analysis of modes for consecutive years (according to Table 2) shows that for any year t with mode M_t = S, the probability for the fast ice to be in mode S the succeeding year, is $P(M_{t+1} = \mathrm{S}|M_t = \mathrm{S}) = 0.67$. Equations (3)–(6) summarize this simple Markov analysis:

$$P(M_{t+1} = \mathrm{S}|M_t = \mathrm{S}) = 0.67 \quad (3)$$

$$P(M_{t+1} = \mathrm{L}|M_t = \mathrm{S}) = 0.33 \quad (4)$$

$$P(M_{t+1} = \mathrm{S}|M_t = \mathrm{L}) = 0.30 \quad (5)$$

$$P(M_{t+1} = \mathrm{L}|M_t = \mathrm{L}) = 0.70 \quad (6)$$

[55] This simplification seems to reflect known interannual climatic variations in the Arctic. Such variations are found in various meteorological, ice and oceanographic parameters [*Mysak and Manak*, 1989]. Note the long period of S mode from 1982 to 1989 and an overall prevalence of this mode during the last 23 years, fitting into the pattern of warmer climate and a more intensive meridional heat and moisture transport during this time [*Rogers and Mosley-Thompson*, 1995; *Walsh et al.*, 1996]. The 10 L-mode years in 1964–1975 similarly occur in the well-documented period of cooling of the Arctic [*Polyakov et al.*, 2003]. The fast ice extent in the Kara Sea during 2002 did not fall into the typical categories as described above (marked "unclassified" in Table 2). The fast ice extent in 2002 never stabilized at islands far from the mainland, as discussed in defining the modes. This had not happened since the observations started in 1953 and it occurred in a year when the ice cover was at its minimum in September since satellite passive microwave observations began in 1978 [*Serreze et al.*, 2003].

[56] The fast ice extent seems to correlate well with large-scale climate variations. A general decline in the Arctic ice cover thickness and extent, as well as intensification of cyclonic circulation, may result in a more frequent S-mode

fast ice extent. The islands that normally support the fast ice far from the mainland may have this role less frequently and the fast ice cover may therefore possess a stable configuration similar to that observed in 2002. This possible outcome may have some direct interest for marine navigation in the area.

[57] **Acknowledgments.** The Norwegian Research Council supported this work via project 128087/730. The International Arctic Research Center, UAF, partly supported participation of A. Makshtas in the framework of Frontier Research System for Global Change. The archive of weather observations at the Dikson Island meteorological station was prepared under the framework of the "Transport and Fate of Contaminants in the Northern Seas" program hosted by the Norwegian Polar Institute. The authors also thank Pål Erik Isachsen and Chad Dick for improvement of the manuscript and S. Divina for preparing Figures 1 and 2.

References

Borodachev, V., Z. Gudkovich, S. Klyachkin, and V. Smolyanitsky (2000), Fast ice conditions in the Kara Sea and possible reasons of interannual changes of fast ice area, in *Transport and Fate of Contaminants in the Northern Seas*, *AARI Final Report*, chap. 1, pp. 3–16, Norw. Polar Inst., Tromsø.

Chaudhuri, P., and J. Marron (1999), SiZer for exploration of structures in curves, *JASA J. Am. Stat. Assoc.*, *94*, 807–823.

Dethleff, D., P. Loewe, and E. Kleine (1998), The Laptev Sea flaw lead: Detailed investigation on ice formation and export during 1991/1992 winter season, *Cold Reg. Sci. Technol.*, *27*, 225–243.

Divine, D. (2003), Peculiarities of shore-fast ice formation and destruction in the Kara Sea, Ph.D. thesis, Univ. of Bergen, Bergen, Norway.

Divine, D., R. Korsnes, and A. Makshtas (2003), Variability and climate sensitivity of fast ice extent in the north-eastern Kara Sea, *Polar Res.*, *22*(1), 27–34.

Divine, D., R. Korsnes, and A. Makshtas (2004), Temporal and spatial variations of shore-fast ice in the Kara Sea, *Cont. Shelf Res.*, *24*(15), 1717–1736.

Eicken, H., T. Viehoff, T. Martin, J. Kolatschek, V. Alexandrov, and E. Reimnitz (1995), Studies of clean and sediment-laden ice in the Laptev Sea, *Rep. Polar Res.*, *176*, 62–70.

Fetterer, F., and V. Troisi (1997), AARI 10-day Arctic Ocean EASE-grid sea-ice observations, http://nsidc.org/, Natl. Snow and Ice Data Cent., Boulder, Colo.

Korsnes, R., O. Pavlova, and F. Godtliebsen (2002), Assessment of potential transport of pollutants into the Barents Sea via sea ice: An observational approach, *Mar. Pollut. Bull.*, *44*, 861–869.

Kozo, T. (1983), Initial model results for Arctic mixed layer circulation under a refreezing lead, *J. Geophys. Res.*, *88*, 2926–2934.

Maslanik, J., and J. Stroeve (1990 updated 2003), DMSP SSM/I daily polar gridded brightness temperatures (CD-ROM), http://nsidc.org/, Natl. Snow and Ice Data Cent., Boulder, Colo.

Mysak, L., and D. Manak (1989), Arctic sea-ice extent and anomalies, 1953–1984, *Atmos. Ocean*, *27*(2), 376–405.

Pavlov, V., and V. Stanovoy (2001), The problem of transfer of radionuclide pollution by sea ice, *Mar. Pollut. Bull*, *42*, 319–323.

Pease, C. (1987), The size of wind-driven coastal polynyas, *J. Geophys. Res.*, *92*, 7049–7059.

Pfirman, S., J. Kogler, and I. Anselme (1995), Coastal environments of the western Kara and eastern Barents Seas, *Deep Sea Res., Part II*, *42*(6), 1391–1412.

Pfirman, S., R. Colony, D. Nurnberg, H. Eicken, and I. Rigor (1997a), Reconstructing the origin and trajectory of drifting Arctic sea ice, *J. Geophys. Res.*, *102*, 12,575–12,586.

Pfirman, S., J. Kogler, and I. Rigor (1997b), Potential for rapid transport of contaminants from the Kara Sea, *Sci. Total Environ.*, *202*, 111–122.

Polyakov, I., R. Bekryaev, G. Alekseev, U. Bhatt, R. Colony, M. Johnson, A. Makshtas, and D. Walsh (2003), Variability and trends of air temperature and pressure in the maritime Arctic, 1875–2000, *J. Clim.*, *16*, 2067–2077.

Reimnitz, E., J. Marincovich, M. McCormick, and W. Briggs (1992), Suspension freezing of bottom sediment and biota in the Northwest Passage and implications for Arctic Ocean sedimentation, *Can. J. Earth Sci.*, *29*, 693–703.

Reimnitz, E., H. Kassens, and H. Eicken (1995), Sediment transport by Laptev Sea ice, *Rep. Polar Res.*, *176*, 71–77.

Rigor, I., and R. Colony (1997), Sea ice production in the Laptev Sea, *Sci. Total Environ.*, *202*, 89–110.

Rogers, J., and E. Mosley-Thompson (1995), Atlantic Arctic cyclones and the mild Siberian winters of the 1980s, *Geophys. Res. Lett.*, *22*, 799–802.

Serreze, M. (1996), Arctic cyclone track data set (1966–1993), http://nsidc.org/, Natl. Snow and Ice Data Cent., Boulder, Colo.

Serreze, M., et al. (2003), A record minimum arctic sea ice extent and area in 2002, *Geophys. Res. Lett.*, *30*(3), 1110, doi:10.1029/2002GL016406.

Sheather, S., and M. Jones (1991), A reliable data-based bandwidth selection method for kernel density estimation, *J. R. Stat. Soc., Ser. B*, *53*, 683–690.

Timokhov, L. (1994), Regional characteristics of the Laptev and the East Siberian seas: Climate, topography, ice phases, thermohaline regime, circulation, *Rep. Polar Res.*, *144*, 15–31.

Volkov, V., O. Johannessen, V. Borodachev, G. Voinov, L. Pettersson, L. Bobylev, and A. Kouraev (2002), *Polar Seas Oceanography: An Integrated Case Study of the Kara Sea*, Springer, New York.

Walsh, J., W. Chapman, and T. Shy (1996), Recent decrease of sea level pressure in the central Arctic, *J. Clim.*, *9*, 480–486.

Weeks, W. (1994), Possible roles of sea ice in the transport of hazardous material, *Arct. Res. U.S.*, *8*, 34–52.

Zubov, N. (1945), *Arctic Ice* (in Russian), Izd. Glavsevmorputi, Moscow. (English translation, U. S. Navy Oceanogr. Off., Stennis Space Center, Miss., 1963.)

Zyryanov, D., D. Divine, and R. Korsnes (2002), Mechanical simulation of shore fast ice breakup: Kara and Laptev seas, paper presented at the International Workshop on Small-Scale Sea Ice-Ocean Modeling for Nearshore Beaufort and Chukshi Seas, Int. Arctic Res. Cent., Fairbanks, Alaska, 8–9 Aug.

D. V. Divine, Norwegian Polar Institute, Polar Environmental Centre, N-9296 Tromsø, Norway. (dmitry.divine@npolar.no)

F. Godtliebsen, Faculty of Science, University of Tromsø, N-9037 Norway. (fred@stat.uit.no)

R. Korsnes, Division for Electronics, Norwegian Defense Research Establishment, Postboks 25, N-2027 Kjeller, Norway. (reinert.korsnes@ffi.no)

A. P. Makshtas, International Arctic Research Center, University of Alaska Fairbanks, 930 Koyukuk Drive, P. O. Box 757340, Fairbanks, AK 99775-7335, USA. (makshtas@iarc.uaf.edu)

H. Svendsen, Geophysical Institute, University of Bergen, Allégaten 70, N-5007 Bergen, Norway. (harald.svendsen@gfi.uib.no)